

1 Increase in late Neogene denudation of the European Alps 2 confirmed by isoage analysis of a fission-track database

3 A.J. Vernon ^{(1,2)*}, P.A. van der Beek ⁽²⁾, H.D. Sinclair ⁽¹⁾, M.K. Rahn ⁽³⁾

4 (1) School of Geosciences, Grant Institute, University of Edinburgh, Edinburgh EH9-3JW, United-Kingdom

5 (2) Laboratoire de Géodynamique des Chaînes Alpines, Université Joseph Fourier, 38400 Grenoble, France

6 (3) Swiss Federal Nuclear Safety Inspectorate, 5232 Villigen-HSK, Switzerland

7 * Corresponding author: antoine.vernon@ed.ac.uk

8

9 **Abstract**

10 A sharp increase in deposited sediment volume since Pliocene times has been observed
11 worldwide and in particular around the European Alps. This phenomenon has been linked to a
12 rise in denudation rates controlled by an increase of either climatic or tectonic forcing.
13 Observation of in situ cooling histories for orogens is critical to assess the reality of the
14 inferred increase in denudation rates, and to determine whether this phenomenon is
15 widespread or localized at active tectonic structures. We exploit the unique density of fission
16 track ages in the Western European Alps to reconstruct cooling isoage surfaces and to
17 estimate exhumation rates on the orogen scale between 13.5 and 2.5 Ma. Our novel technique
18 is based on the association of isoage contours with age-elevation relationships. It uses map-
19 view interpolation, enabling a spatio-temporal analysis of exhumation rates over the entire
20 Western Alps. The resulting exhumation histories reconstructed for eight areas of the Western
21 Alps display strong similarities in timing and rates with orogen-wide average denudation rates
22 inferred from sediment volumes. This consistency validates the use of both techniques for the
23 study of an orogen characterized by strong relief and high recent exhumation rates. We
24 conclude that exhumation rates in the Western Alps have increased more than twofold since

25 late Miocene times. This increase may have been locally modulated by the distinct response
26 of different tectonic units.

27

28 Keywords: Cenozoic exhumation, Fission track, Isoage surfaces, Western Alps

29

30 **1. Introduction**

31 Widespread indications for an increase of global sedimentation rates in the early Pliocene
32 have been reported from localities around the world (e.g., Molnar, 2004; Zhang et al., 2001).

33 However, the cause of this event, its exact timing and synchronicity remain controversial.

34 Possible causes that have been proposed include global cooling and incipient glaciations
35 (Ehlers et al., 2006; Hinderer, 2001), an increase in the magnitude and frequency of climate
36 oscillations (Molnar, 2004; Zhang et al., 2001), and a recent increase in the uplift rates of
37 major orogens (Raymo and Ruddiman, 1992).

38

39 The quantification of sediment volumes in the basins surrounding the European Alps by
40 Kuhlemann et al. (2002) shows a more than twofold increase in erosion rates in both the
41 Western and Eastern Alps around 5 Ma (Figure 1). An independent study of the exhumation
42 of the Molasse basin (Figure 2), based on borehole apatite fission-track data, demonstrated
43 approximately 1400 m of basin exhumation since 5 Ma, interpreted as a record of isostatic
44 rebound of the basin driven by accelerated erosional unloading of the Alps (Cederbom et al.,
45 2004).

46

47 The estimation of source-area denudation rates from the sediment record suffers, however,
48 from poorly quantified uncertainties in both the volumetric calculations and the dating
49 accuracy (Kuhlemann et al., 2002). Moreover, the impossibility of quantifying the roles of

50 chemical erosion and sediment recycling may lead to an underestimation or overestimation,
51 respectively, of source-area denudation rates.

52

53 An increase in exhumation at ca. 5 Ma, if real, should be recorded more directly by low-
54 temperature thermochronometers in the bedrock of the mountain belt. Classically, the
55 derivation of exhumation rates from thermochronometry is based on temperature-time paths
56 reconstructed from multiple thermochronometer analysis, age-elevation profiles from
57 altitudinal transects or boreholes, or kinetic modeling of apatite fission-track annealing using
58 track-length distributions (e.g., Gallagher et al., 1998; Hurford, 1991). In different regions of
59 the Western Alps, Neogene-age exhumation rates quantified using these approaches range
60 between 0.1 and 1.5 mm/yr (e.g., Leloup et al., 2005; Malusa et al., 2005; Michalski and
61 Soom, 1990; Tricart et al., 2007). However, most of these studies are local or at best regional
62 in scope and a consistent denudation history at the orogen scale has yet to emerge. Apatite
63 fission-track (AFT) thermochronology appears the most suitable technique to study Mio-
64 Pliocene exhumation rates over a large area such as the Western Alps because of the
65 abundance of ages ready for database compilation, and because the AFT age range (Figure 3-
66 a) comprises the target period of the late Neogene.

67

68 The spatial integration of discrete thermochronological data covering large study areas is most
69 easily achieved by interpolating between ages in map view (e.g., Hunziker et al., 1992;
70 Figures 3-a and 3-b). However, this simple technique only presents the integrated result of a
71 possibly complex denudation history and does not allow variations in denudation rate through
72 time to be inferred. Published methods aimed at describing the history of exhumation rates in
73 map view have used either analysis of multiple thermochronometers, or kinetic modeling of
74 fission-track length distributions (e.g., Bistacchi and Massironi, 2000; Gallagher and Brown,

75 1999; Morris et al., 1998; Schlunegger and Willet, 1999; Stephenson et al., 2006). Despite
76 many years of intensive thermochronological studies in the Alps, samples permitting such
77 analyses are still relatively rare, disallowing such a study at the orogen scale. Techniques
78 based on modeling of fission-track length distributions offer the greatest wealth of
79 interpretation in settings characterized by slow long-term denudation, such as rifted
80 continental margins (e.g. Gallagher and Brown, 1999). In rapidly exhuming orogens, in
81 contrast, track-length distributions are not easily measured (because of generally young AFT
82 ages) and are much less discriminative.

83
84 We propose a new method in which we exploit the extensive AFT dataset available for the
85 Western Alps (Figures 2 and 3) together with the significant relief of the mountain belt to
86 reconstruct three-dimensional surfaces of equal AFT age (referred to here as isoage surfaces).
87 We subsequently use the difference in elevation between these surfaces to estimate the spatial
88 pattern in rates of exhumation back to middle Miocene times (13.5 Ma), as recorded in the
89 spatial relationship between AFT ages at outcrop today. The aims of this study are to test for
90 the presence of changing exhumation rates during late Neogene times across the Western
91 Alps, and if present, to describe the temporal and spatial variability of this signal. In addition,
92 we present updated maps of interpolated apatite fission-track ages and mean track lengths, as
93 well as zircon fission-track ages. We complete this study by the assessment of evolving trends
94 of exhumation rates using samples with paired zircon and apatite fission-track ages. In the
95 following, we first briefly outline the geological setting and evolution of the Alps and present
96 the thermochronological database we constructed. We then explain the different methods we
97 used to analyze the database. Finally, we present our main results and their implications for
98 the late Neogene denudation history of the Alps as well as its possible tectonic or climatic
99 controls.

hal-00286544, version 1 - 9 Jun 2008

100
101
102
103
104
105
106
107
108
109
110
111
112
113
114
115
116
117
118
119
120
121
122
123
124

2. Geological setting of the Alps

The European Alps (Figure 2) are located at the boundary between the European and Apulian plates. They are the product of the early Cretaceous closure of the Piemont-Ligurian ocean, followed by continental subduction resulting in nappe stacking (cf. reviews in Rosenbaum and Lister, 2005; Schmid et al., 2004).

The main tectonic units in the Alps and their structural relationships have been described extensively within the last century (e.g., Debelmas and Lemoine, 1970; Schmid et al., 2004; Trümpy, 1960). They originate from the European continental margin basement (External Crystalline Massifs) and overlying deposits (Helvetic sediments), the Briançonnais micro-continent and its two bordering oceanic units (Piemont-Ligure and Valais oceanic crust and flysh), and finally basement and sedimentary units of the Apulian margin, grouped as the Austroalpine and the South Alpine units (Figure 2). The North (Molasse) and South (Po) Alpine foreland basins formed by flexure of the lithosphere in response to the weight of the orogenic prism on the European and Apulian plates and are filled with Eocene to Recent flysch, molasse and glacial deposits (e.g., Homewood et al., 1986; Scardia et al., 2006).

One of the most important arc-parallel tectonic boundaries, the Penninic thrust, may have been extensionally reactivated (Seward and Mancktelow, 1994) as part of a series of Neogene extensional features observed throughout the axial region of the Western Alps (e.g., Sue et al., 2007; Tricart et al., 2007 and references therein). Most of these extensional features may be caused by a Neogene dextral transtensive event (Sue et al., 2007) triggered by the anti-clockwise rotation of the Apulian plate. Such rotation can also explain the current strain pattern in the Western Alps (Calais et al., 2002). At present, geodetic and GPS data show

125 limited (≤ 2 mm/yr) east-west extension in the Western Alps (Calais et al, 2002; Sue et al.,
126 2007). The lack of present-day convergence in the Western Alps, together with the
127 observation of sediment-sealed thrusts in the western part of the Po basin (Pieri and Groppi,
128 1981), and the cessation of thin-skinned deformation in the Jura at ca. 4 Ma (Becker, 2000) all
129 suggest very limited current orogenic activity within the chain.

130

131 We limit our study area to the Western half of the Alps, as far east as the Silvretta nappe /
132 Engadine window, or approximately the Swiss-Austrian border, which marks the western
133 limit of widespread outcrop of Austroalpine units. The reason for this eastern limit to the
134 study area is that few AFT studies have been published for the Austroalpine units because of
135 the low abundance of apatite in their constitutive lithologies.

136

137 **3. Data**

138 **3.1. Apatite and zircon fission-track databases**

139 During the last thirty-five years, the Western Alps have been extensively sampled for
140 thermochronological analyses, in particular using the apatite and zircon fission-track
141 thermochronometers, characterized by closure temperatures of ca. 120 and 240 °C
142 respectively (e.g., Brandon et al., 1998; Gallagher et al., 1998). We have compiled 740 AFT
143 ages, from data in 37 publications completed by 160 unpublished ages (references are given in
144 the caption of Figure 3-a) from samples located in the European Alps west of 10° 20' east (an
145 area of ca. 48000 km²). We similarly compiled 380 zircon fission-track (ZFT) ages from 24
146 publications completed by 22 unpublished ages (see Figure 3-b for references).

147

148 3.2. Quality and homogeneity of the data

149 Early studies (in the 1970's and early 1980's, see for instance Wagner and Reimer, 1972)
150 used the population method for AFT dating, whereas the more reliable external detector
151 method (Hurford and Green, 1982) has become the norm since the mid 1980's. The database
152 contains ages obtained both with the population and the external-detector dating techniques
153 because we feel that, at the regional scale of the study, the benefits of increasing data density
154 outweigh the drawbacks of the error introduced by less reliable data points. We rejected three
155 samples with an obvious mistake in dating, in cases where a ZFT age was younger than or
156 equal to (within error) the AFT age of the same sample.

157
158 Additional information collected for each sample included (where reported): (1) geographic
159 coordinates, (2) elevation, (3) mean track length for AFT samples, (4) whether the sample is
160 from a tunnel / borehole or the surface, and (5) whether fission-track ages of samples from
161 Mesozoic and Cenozoic sediments are younger than their stratigraphic age (that is, whether
162 they have been reset during Alpine orogeny). To apply the latter criterion, we assumed that
163 ages from sedimentary samples were non-reset unless we could estimate the depositional age
164 and verify that it was older than the fission-track age. A few publications contained more than
165 one age at a given geographic location (referred to later as points with non-unique ages). We
166 discarded such points from part of the study, in order to prevent problems with map
167 interpolation. Many of the original publications did not report sample elevations and / or
168 coordinates. We obtained this missing information by interviewing the authors whenever
169 possible, or alternatively by reading it off topographic maps or figures from the original
170 publications. As a last resort, we estimated the elevation of samples from the Digital
171 Elevation Model (DEM), which consists of a mosaic of the 38-03, 38-04, 39-03 and 39-04
172 DEM tiles available from the CGIAR-CSI SRTM 90 m database (<http://srtm.csi.cgiar.org>).

hal-00286544, version 1 - 9 Jun 2008

173 All numerical data fields in the database (coordinates, altitude, age, etc.) carry a degree of
174 uncertainty that varies between publications. For instance, the relative standard errors
175 affecting the AFT and ZFT ages used in this paper vary between 2.2 and 51.6 % (average:
176 11.6 %) for the former, and between 0.7 and 23.3 % (average 8.0 %) for the latter.

178 **4. Methods**

179 We have developed three joint approaches to take advantage of the high spatial density of
180 fission-track ages in the Western Alps. First, we interpolated AFT and ZFT ages (Figures 3-a
181 and 3-b); second, we calculated cooling and exhumation rates using samples dated with both
182 methods; and third, we constructed isoage surfaces. The latter were used to infer histories of
183 exhumation rates for different areas of the Western Alps between 13.5 and 2.5 Ma.

185 **4.1. Maps of interpolated ages / track lengths**

186 Using the natural-neighbor interpolation tool provided by the ESRI-ArcMap9tm GIS, we
187 created two maps of 635 AFT ages and 296 ZFT ages covering the Western Alps (Figures 3-a
188 and 3-b). For this interpolation, we selected points from the database following three criteria:
189 (1) ages in sedimentary rocks should be reset; (2) samples should be from the surface; and (3)
190 points with non-unique ages are discarded. No potentially arbitrary constraints such as
191 tectonic boundaries or elevation corrections were used in this initial interpolation. The choice
192 of a natural-neighbor interpolator is justified by its conservative properties, resulting in
193 finding at each pixel of the map a weighted average of the neighborhood data points without
194 introducing artefacts (Watson, 1999). However, as we could not introduce a maximum
195 distance of interpolation, localities within the inner Alpine arc are often interpolated between
196 data points located very far apart, at two extremities of the arc. Figure 3-c shows a map of 258
197 mean AFT lengths, interpolated in the same manner as the ages.

198
199
200
201
202
203
204
205
206
207
208
209
210
211
212
213
214
215
216
217
218
219
220
221
222

4.2. Exhumation rates calculated from paired ZFT and AFT ages

We extracted from the database a subset of 143 samples with paired AFT and ZFT ages, following the requirements that (1) they are surface samples; (2) both AFT and ZFT ages are younger than 35 Ma (i.e., Alpine cooling ages); (3) AFT and ZFT ages differ by at least 1.6 Myr (an empirical limit set by convergence problems for smaller age differences in the numerical code used); finally (4) points with non-unique ages are discarded. The 143 age pairs offer the opportunity to estimate two successive average exhumation rates: an initial rate during the time between closure of the ZFT and AFT thermochronometers, and a final rate for the time since closure of the AFT system. We used a modified version of the one-dimensional model of Brandon et al. (1998) to calculate iteratively the depth of closure of the ZFT and AFT systems, and then calculate exhumation rate from the value of closure depth and age. This model takes into account the advective perturbation of a steady-state geotherm by exhumation, as well as the dependence of closure temperature on cooling rate (e.g., Dodson 1973). It does not, however, include 2-D or 3-D effects such as non-vertical rock-particle paths, spatial variation in geothermal gradient or topographic effects. We have adapted the Brandon et al. (1998) model to simultaneously estimate closure temperatures and depths for both the ZFT and AFT systems (cf. Braun et al., 2006 and van der Beek et al., 2006 for details), using values for the kinetic parameters as estimated by Brandon et al. (1998): AFT: $E_a = 186.4 \text{ kJ mol}^{-1}$, $D_0/a^2 = 3.64 \times 10^{10} \text{ s}^{-1}$; ZFT: $E_a = 208.2 \text{ kJ mol}^{-1}$, $D_0/a^2 = 3.70 \times 10^6 \text{ s}^{-1}$. Other parameter values used in the model are: surface temperature $T_s = 15 - (6 \times \text{elevation (km)}) \text{ }^\circ\text{C}$, initial (non-perturbed) geothermal gradient $G = 25 \text{ }^\circ\text{C km}^{-1}$, model thickness $L = 25 \text{ km}$, thermal diffusivity $\kappa = 25 \text{ km}^2 \text{ Myr}^{-1}$. The model predicts initial and final exhumation rates that are consistent with both ages; the ratio between the final and initial rates indicates whether the average exhumation rate accelerated or decelerated after closure of the AFT

223 system. An interpolated map of this ratio is plotted in Figure 4. Absolute values of predicted
224 exhumation rates are affected by the assumed initial geothermal gradient, which is largely
225 unknown and may vary spatially. However, the *ratio* between final and initial rates is not
226 sensitive to this parameter, providing the geothermal gradient does not change through time,
227 other than through advective perturbation.

228

229 **4.3. Reconstruction of isoage surfaces**

230 Apatite fission-track isoage surfaces join all rocks predicted to have cooled through the AFT
231 closure temperature at the same time (Figure 5). They are obtained by interpolation in map
232 view between the elevations of points having the same AFT age. Providing the assumption
233 that the depth of the AFT closure isotherms is only moderately affected by changes in
234 exhumation rate, the latter can be estimated using the vertical distance between two
235 successive isoage surfaces. In this respect, isoage surfaces may be viewed as a 3-D
236 generalization of the 1-D age-elevation profile concept, allowing the same information on
237 denudation history to be extracted on a regional scale and potentially recording spatial
238 variations in denudation rates through time.

239

240 Regional variability in geothermal gradient, cooling history and / or apatite annealing kinetics
241 may cause the closure temperature and depth to vary spatially between samples from different
242 tectonic units, thus potentially imposing secondary effects on the spatial variation in elevation
243 of isoage surfaces. However, as for age-elevation profiles, the denudation rate inferred from
244 the elevation difference between successive isoage surfaces is independent of the absolute
245 closure temperature and depth, as long as these remain constant through time. Temporal
246 variations in exhumation rates may affect the AFT closure temperature (Dodson, 1973) as
247 well as the geometry of near-surface isotherms (e.g., Braun, 2002; Stüwe et al., 1994). These

248 two factors tend respectively toward over- or under-estimation of the exhumation rate in the
249 case of an increase in exhumation rate. Nevertheless, the characteristic diffusive timescales
250 are rather large (e.g., Braun et al., 2006) so that these variations will be relatively small over
251 the 1 Myr time span separating two isoage surfaces. In any case, the latter effect significantly
252 outweighs the former (e.g., Braun et al., 2006), so that estimated exhumation rates during a
253 period of increase before reaching a thermal steady-state are likely to be minimum estimates.

254

255 **4.3.1. Production of arrays of isoage points**

256 The most obvious way to obtain x, y, z coordinates of isoage points is to use the elevation of
257 isoage contours, which, by definition, are the lines of intersection between isoage surfaces and
258 the Earth's surface. We extracted the elevation of each isoage contour traced on the maps of
259 interpolated AFT ages (Figure 3-a) by projection on the Digital Elevation Model (DEM). The
260 spatial resolution of the DEM (90 m) is much higher than the resolution of the isoage contours
261 (controlled by interpolated points often separated by several kilometers). Therefore, the
262 elevation of any segment of an isoage contour has a high pixel-to-pixel variability (or noise)
263 due to the short-wavelength topography sampled. Nevertheless, the average local value should
264 accurately reflect the elevation of the intersection between an isoage surface and the
265 topography.

266

267 We added a second series of isoage points to the array, based on local estimates of AFT age-
268 elevation relationships (AER) in the neighborhood of data points where the correlation
269 between these two parameters was statistically significant (Figure 6). The aim is to document
270 areas where the AER are well correlated and use them to interpolate the elevation of isoage
271 surfaces. We used a subset of 660 AFT samples with an age younger than 35 Ma for this
272 approach. Sample elevation values that had to be derived from the DEM were found to

273 introduce too much noise in the calculation of regression coefficients for age-elevation
274 relationships and were therefore rejected. We did include, however, data points with non-
275 unique ages, as they comply with the requirements to estimate age-elevation relationships.
276 The condition of sample ages younger than 35 Ma aims to avoid introducing samples that are
277 manifestly partially reset, such as those with Mesozoic ages from the Southern Alps (cf.
278 Figure 3-a), into the calculation of AER regression lines.

279
280 For our semi-automated AER analysis, we first selected the neighbors of every point in the
281 database, included in a circle of increasing radius (from 3 to 15 km). For every selection
282 containing more than 4 points, we calculated a regression line between age (dependent
283 variable) and elevation (independent variable), together with its correlation coefficient. The
284 AER was judged significant and was retained if the correlation coefficient for the regression
285 was higher than the critical Pearson's product-moment coefficient at 95 % confidence level
286 for the appropriate number of degrees of freedom (cf. Figures 6-b and 6-c). When the initial
287 selection around a data point (3 km radius) failed this statistical test, we incrementally
288 increased the search radius by 2 km steps to a maximum of 15 km. This maximum presents a
289 characteristic distance between adjacent valleys: for larger search radii, the samples selected
290 may belong to adjacent valleys with distinct exhumation histories. We used the regression
291 equations calculated from the set of points selected within the smallest successful search
292 radius possible, because they constitute the closest equivalent to a vertical profile and
293 therefore carry the smallest risk for the AER to be affected by either large-scale tilting (Rahn
294 et al., 1997) or the deflection of isotherms in large Alpine valleys (e.g., Braun, 2002; Stüwe et
295 al., 1994).

296

297 The local AER is described by the simple linear equation $z = A_0 + (A_1 \times t)$, where A_0 is the
298 elevation of the zero-age intercept, and A_1 is the slope of the AER (with z : elevation [m]; t :
299 age [Ma]). Statistically significant AERs extracted from the data are used to interpolate the
300 elevations of isoage surfaces at the location of the center of the search radius, limiting the
301 extrapolation to between 1 Myr before the oldest and 1 Myr after the youngest age in the
302 neighborhood selection. This limitation is imposed in order to avoid extrapolating age-
303 elevation trends into periods during which they are not locally documented. In case of a
304 slightly kinked AER (i.e. change in exhumation rate with time), the slope A_1 would be
305 averaged; if the kink is more pronounced the linear correlation coefficient will be insignificant
306 and the neighborhood selection rejected. Given that this study is aimed at testing for changing
307 exhumation rates through time, the rejection of kinked AERs in the generation of isoage data
308 points is conservative, and will downplay any signal.

309

310 **4.3.2. Interpolation of isoage point arrays**

311 We constructed isoage surfaces by natural-neighbor interpolation applied to the elevations of
312 the points constituting each isoage array (Figure 6d). In order to remove unconstrained parts
313 of the surfaces, which have been interpolated far from any point of the isoage arrays, a mask
314 is applied at 15 km around the point arrays. The oldest isoage surfaces have been eroded from
315 large parts of the study area, while the youngest surfaces remain buried in other areas,
316 resulting in a heterogeneous scatter of each array of isoage points. The result is a series of
317 thirteen maps showing isoage surfaces between 14 and 2 Ma where they can be reconstructed
318 with reasonable accuracy; a representative selection of six isoage surfaces is reported in
319 Figure 7.

320

321 **4.4. Estimation of exhumation rates**

322 The vertical distance between two isoage surfaces corresponds, in principle, to the amount of
323 exhumation during the time period separating them, with the same caveats that apply to the
324 interpretation of 1-D age-elevation profiles, notably the effect of topography on the AER
325 slope (Braun, 2002). In the crystalline massifs of the Western Alps, geomorphic data suggest
326 a significant recent increase in relief (e.g., Champagnac et al., 2007; van der Beek and
327 Bourbon, 2008) so that we expect topographic effects to be limited and the distance between
328 successive isoage surfaces to provide a reliable estimate of exhumation.

329

330 After being clipped by the 15 km mask, each isoage surface covers only a limited portion of
331 the Western Alps, and two successive surfaces are never completely superposed. Therefore, it
332 is not possible to calculate the total volume exhumed over the entire surface of the Western
333 Alps during any time period. Instead, we focused on eight specific areas characterized by
334 several million years of continuous isoage surface coverage (Figure 8).

335

336 The difference in elevation between successive isoage surfaces is calculated for all 1.2 km²
337 pixels of each study area and the average distance constitutes our estimate of exhumation
338 during the corresponding time period. Some pixels show negative differences, i.e. the younger
339 isoage surface lies above the older one. These correspond either to artefacts introduced by our
340 treatment of the data or to local areas of strong recent relief decrease. We decided to exclude
341 these pixels from our calculation of the average distance between isoage surfaces, as two
342 isoage surfaces cannot cross each other in an exhuming massif. To illustrate pixel value
343 distributions, Figure 9 presents the values measured between the surfaces aged 5 and 4 Ma for
344 the Mont Blanc area. Plotted against time, the average distances between isoage surfaces
345 enable quantifying the temporal evolution of exhumation rates over each area (Figure 10).

hal-00286544, version 1 - 9 Jun 2008

346
347
348
349
350
351
352
353
354
355
356
357
358
359
360
361
362
363
364
365
366
367
368
369

Samples that underwent slow cooling through the partial annealing zone may lead to apparent AERs that do not correspond to the exhumation rate (e.g., Gallagher et al., 1998). The mean track lengths can be used to monitor whether this is the case, as samples that cooled slowly through the partial annealing zone are characterized by mean track length $\leq \sim 12.5 \mu\text{m}$. Most areas covered by our constructed isoage surfaces are characterized, in contrast, by sample mean track length $\geq 13 \mu\text{m}$ (compare Figures 3-c and 8), with the exception of the Bergell and the Aar-Leventina (areas 1 and 6 in Figure 8).

5. Results

5.1. Main features of the fission-track age patterns

Young AFT ages ($< 10 \text{ Ma}$) appear in the axial region of the Western Alps (Figure 3-a) and particularly over the Argentera, Ecrins - Mont-Blanc, and Aar External Crystalline Massifs. Very young ages ($< 5 \text{ Ma}$) are also found in the Chur region, between the eastern Aar and the Silvretta nappe, and in the western Lepontine dome, east of the Simplon fault. In contrast, the internal crystalline massifs (Gran Paradiso, Dora Maira) as well as the Austroalpine units are characterized by early Miocene or older AFT ages ($> 10 \text{ Ma}$). An inverse relationship between AFT age and mean track length appears, with ages $< 10 \text{ Ma}$ generally characterized by mean track length $> 13 \mu\text{m}$ (compare Figures 3-a and 3-c). The only exception to this pattern is a band of short mean track lengths extending from the central Aar massif to the SSE (Figure 3-c). Young ZFT ages ($< 15 \text{ Ma}$) characterize the Aar, Mont-Blanc, Belledonne and Lepontine massifs (Figure 3-b). Extensive regions of both the external and internal parts of the orogen show early Alpine ZFT ages (20-35 Ma), whereas two orogen-parallel bands (an external band covering the frontal parts of the Mont-Blanc and Aar massifs and an internal

hal-00286544, version 1 - 9 Jun 2008

370 band running from the eastern Ecrins across the Southern Alps) show ZFT ages that were not
371 reset by the Alpine orogeny (i.e., ZFT age \geq 35 Ma).

372
373 The AFT and ZFT age patterns run parallel to two major Alpine tectonic lineaments: the
374 Penninic thrust, bordering the External Crystalline Massifs, and the Simplon fault. Both areas
375 show younger ages in their footwalls (Figures 3-a and 3-b), which suggests that a component
376 of tectonic exhumation may affect the age patterns, as previously suggested in more local
377 studies (Fügenschuh and Schmid, 2003; Seward and Mancktelow, 1994; Tricart et al., 2007).

378
379 **5.2. Variation in exhumation rate from paired AFT and ZFT ages**

380 A pattern of recent accelerated exhumation, dominantly affecting the external side of the belt
381 (and the External Crystalline Massifs in particular), is evidenced in Figure 4. This map
382 demonstrates an overall acceleration in exhumation rate along the northern and western
383 borders of the orogen, since these areas crossed the AFT closure temperature of \sim 120 °C.
384 AFT ages in the region showing accelerated denudation are mostly \leq 8 Ma (compare Figures
385 3-a and 4). However, exhumation rates used in this ratio calculation are average values for
386 initial cooling between the ZFT and AFT closure temperatures and final cooling between the
387 AFT closure temperature and the surface, and do not enable us to resolve when the
388 acceleration occurred.

389
390 **5.3. Description of isoage surfaces**

391 The elevation of isoage surfaces generally increases with age (see legend on each map of
392 Figure 7), which is consistent with the assumption that isoage surfaces are mainly controlled
393 by the effect of denudation on isotherms (Figure 5). The overall shape of the isoage surfaces
394 is that of arcuate domes, the axes of which are roughly superposed with the External

395 Crystalline Massifs (Aar, Mont-Blanc and Ecrins, see Figure 2) for the younger surfaces, and
396 with more internal massifs (Lepontine Alps, Dent-Blanche) for older surfaces. Young isoage
397 surfaces are defined mostly by points from high-relief areas with young fission-track ages in
398 the valleys, whereas old isoage surfaces are controlled by locally old fission-track ages
399 encountered on topographic peaks and the elevation of isoage contours in the periphery of the
400 orogen.

401

402 **5.4. Spatial and temporal evolution of exhumation rates**

403 The difference in elevation of AFT isoage surfaces was used to estimate exhumation rates
404 between 13.5 and 2.5 Ma over the Western Alps (Figures 7-10). Comparing curves of
405 exhumation rate against time for different sub-areas (Figure 10) highlights a series of eight
406 overlapping segments from 9.5 to 2.5, 9.5 to 4.5, 13.5 to 10.5 and 13.5 to 4.5 Ma, which all
407 share a similar trend. The estimates of exhumation rate vary between 200 and 700 m/Myr,
408 with an acceleration centered around 5 Ma, which is in surprisingly good agreement with peri-
409 alpine sedimentation rates and inferred alpine denudation rates reported by Kuhlemann and
410 co-workers (Kuhlemann, 2000; Kuhlemann et al., 2002). While we are mostly interested in
411 the pattern of denudation rates at the orogen scale, regional variations in the exhumation
412 history demonstrate the localization of denudation (Figure 10). The exhumation rates
413 estimated in the Bergell and Valais-Sesia areas (curves 1 and 2) are similar and indicate a
414 denudation rate of ~300 m/Myr between 13.5 and 10.5 Ma. The Ecrins and Mont-Blanc
415 massifs (curves 3 and 4) share a similar pattern of increase in exhumation rate between 5.5
416 and 4.5 Ma, with recent rates reaching 500 m/Myr. Further east, the Aar-Leventina area
417 (curve 6) shows a slightly earlier increase in exhumation rate (~6 Ma). However, the
418 occurrence of short mean track lengths in the Aar-Leventina and the Bergell areas (cf. section
419 4.4) may lead us to overestimate recent exhumation. In contrast, the onset of the acceleration

420 in the Simplon and Chur areas (curves 5 and 7) appears to be younger than 3.5 Ma, with
421 recent denudation rates reaching over 600 m/Myr. The sub-area with the longest continuous
422 coverage in isoage surfaces (area 8 on Figure 8) combines a suite of small areas in the
423 Western Alps. The values of exhumation rate it provides between 13.5 and 4.5 Ma (curve 8 on
424 Figure 10) are included within the range of the seven other sub-areas.

425

426 **6. Discussion**

427 **6.1. Conditions of use of isoage surfaces**

428 The use of isoage surfaces to calculate exhumation rates through time requires that the
429 surfaces have not been significantly deformed. Therefore, actively deforming thrust belts
430 would need to be treated with caution. Locations undergoing relief reduction are also to be
431 avoided because age-elevation relationships would provide overestimates of exhumation rates
432 (Braun, 2002). The optimal conditions are met in orogens where relief is either steady or
433 increasing, and tectonic activity is insufficient to significantly deform the isoage surfaces. The
434 Western Alps are a successful candidate because relief appears to have increased recently due
435 to glaciations (Champagnac et al., 2007; van der Beek and Bourbon, 2008), whereas present-
436 day tectonic activity is limited (e.g., Calais et al., 2002). Moreover, the European Alps are
437 covered by an exceptional density of existing AFT ages, allowing us to use the approach
438 developed here.

439

440 **6.2. Errors affecting exhumation rate calculations**

441 Several types of error potentially affect the calculation of exhumation rates from isoage
442 surfaces: (1) uncertainties affecting the ages, elevations and coordinates of samples in the
443 database used to compute isoage surfaces, (2) heterogeneous scatter of the interpolated data
444 points, and (3) geological factors such as the composition of apatites (defining their precise

445 closure temperature) and spatial or temporal variations in relief and geothermal gradient.
446 While errors of type 1 can be estimated on a sample per sample basis, propagating these into
447 an uncertainty in isoage surface elevation cannot be done rigorously, although a Monte Carlo
448 approach in which the surfaces are created thousands of times while varying the input data
449 within error could be envisaged. Whereas uncertainties of type 2 (role of sampling density and
450 scatter) are generally assessed using kriging techniques, these are limited for geological
451 applications because of strong assumptions on spatial continuity and statistics of the data.
452 Alternatively such errors may be evaluated using calculation-intensive boot-strap techniques.
453 Uncertainties of type 3, however, are practically impossible to quantify. Moreover, the weight
454 of these three types of errors within the final uncertainty in exhumation rates is unknown.
455 Therefore, we chose to present the estimates of exhumation rates as such, without the addition
456 of an inherently partial and, therefore, misleading error.

457

458 **6.3. Comparison between exhumation rates and the volume of sediment deposited** 459 **through time**

460 The exhumation rates calculated from the AFT isoage surfaces over the Western Alps (Figure
461 10) are of the same order (200-600 m/Myr) as those calculated from the sedimentary record
462 (Kuhlemann, 2000; Willett et al., 2006). They are also, more expectedly, comparable with
463 denudation rates obtained from local thermochronological studies (e.g., Michalski and Soom,
464 1990; Schär et al., 1975; Schlunegger and Willett, 1999; Tricart et al., 2007). Thus, both the
465 sedimentary record and the in-situ thermochronological record show a similar increase in
466 exhumation rates around 5 Ma. However, the thermochronometric estimates of denudation
467 rates are overall slightly higher than those obtained from the sedimentary record (Figure 10).
468 This small offset may be explained by the fact that areas with the most complete isoage
469 surface coverage, which are used in the calculations, are biased toward the more rapidly

470 eroding massifs with young AFT ages in the valleys, and therefore do not constitute a
471 representative sampling of the entire Western Alps. Other explanations could be an
472 overestimation of exhumation rates obtained from age-elevation relationships (Braun, 2002)
473 or a general bias in the calculation of sediment volume, which, for instance, does not take
474 chemical weathering or sediment recycling into account.

475

476 **6.4. Possible causes for increased recent exhumation**

477 Over the last 14 Myr, the shift of the apex of isoage surface domes through time from the
478 inner Alps to the External Crystalline Massifs (Figure 7) suggests a shift of the most actively
479 exhuming regions during late Miocene and Pliocene times. This idea is in agreement with the
480 map of the ratio of final / initial exhumation rates (Figure 4), where acceleration of
481 exhumation is observed after AFT closure in the External Crystalline Massifs..

482

483 Within this general frame, we observe a broad increase in exhumation rate in the Western
484 Alps centered around 5 Ma, with local variations in the timing of this increase (Figure 10).
485 Assuming that these variations are significant compared to the unquantified uncertainty, they
486 suggest that the rise in Alpine denudation described as happening around 5 Ma (e.g.
487 Cederbom et al., 2004; Kuhlemann, 2000), actually varied considerably, taking place between
488 6.5 and 2.5 Ma depending on local tectonic and structural conditions. A clear expression of
489 regional diversity within a general trend of exhumation increase is found in the Simplon and
490 Chur areas (Figures 8 and Figure 10). The recent surge in exhumation rates in these areas can
491 be linked spatially to present-day high rock-uplift rates in the western and eastern Aar massif
492 (e.g., Persaud and Pfiffner, 2004). Although a significant part of present-day rock uplift rates
493 could be due to the isostatic response to erosional unloading (Champagnac et al., 2007;
494 Schlunegger and Hinderer, 2001), this spatial link may suggest that these two locations are

495 characterized by high rock uplift rates since at least the time of AFT closure. Furthermore,
496 this pattern suggests that current exhumation of the Aar massif is concentrated on its western
497 and eastern borders, and has been so for several million years.

498
499 Based on the approximate temporal coincidence between Mio-Pliocene acceleration of
500 exhumation in the Western Alps, and the closure of the Panama isthmus and subsequent
501 reorganization of Atlantic Ocean currents, Cederbom et al. (2004) proposed that the increase
502 in exhumation around 5 Ma was externally controlled by increased precipitation over Europe.
503 An alternative, and more global mechanism, is that the increased variability of climate
504 witnessed by the ocean oxygen isotope record forced accelerated erosion rates, although the
505 data suggest that this happened between 4 and 3 Ma (e.g., Molnar, 2004; Zhang et al., 2001).
506 Although this explanation remains difficult to confirm, it is seducing as a cause on a global, or
507 at least a continental, scale could explain the simultaneous increase in exhumation in other
508 orogens (e.g., Molnar, 2004; Zhang et al., 2001). Uplift of the Western Alps followed by
509 widespread exhumation may also be controlled by a deep-seated event such as slab
510 detachment; however, no evidence exists to tie such an event down at this particular time.

511

512 **7. Conclusions**

513 Our analysis of the complete fission-track thermochronology database in the Western Alps
514 leads to the following general conclusions:

515 1) Although different regions of the Western Alps show a variable absolute amount of
516 exhumation since 13.5 Ma, they share a common trend of doubling in exhumation rates at
517 approximately 5 Ma. Providing assumptions on error values, it is possible to distinguish
518 between areas where the rise in Alpine denudation took place at different periods within a 6.5
519 to 2.5 Ma time frame.

520 2) The overall consistency between estimated denudation rates using sediment volumes
521 (Kuhleemann, 2000), and bedrock thermochronology (this study) demonstrates that, although
522 both records are fragmentary and error-prone, they are appropriate to describe the general
523 exhumation history at the orogen scale since at least 13.5 Ma.

524 3) The maps of zircon and apatite fission-track ages share a pattern of young ages over an arc
525 linking the External Crystalline Massifs, as well as in the area of the Lepontine Alps,
526 suggesting that these areas underwent the strongest recent denudation in the Western Alps.
527 The observed longer mean AFT lengths in the areas with young fission track ages further
528 supports this conclusion.

529 4) This pattern fits with the trend of accelerated exhumation rates calculated from samples
530 with paired zircon and apatite fission-track ages. This trend indicates that most of the Western
531 Alps, in particular the external side of the arc, was on average exhumed faster after AFT
532 closure than between the times of ZFT and AFT closure.

533

534 **Acknowledgements**

535 This study is supported by an INSU-CNRS “Reliefs de la Terre” program grant to PvdB. AV
536 is supported by a University of Edinburgh PhD teaching scholarship and an international
537 student mobility (MIRA) grant of the Rhône-Alpes region. We are grateful to M. Ford and D.
538 Seward for permission to use unpublished AFT ages. L. Keller, P. Leloup, S. Schwartz and P.
539 Tricart kindly provided complementary details on their published material. The manuscript
540 benefited from thorough and constructive reviews by Kerry Gallagher and an anonymous
541 reviewer.

542

543 **References**

- 544 Becker, A., 2000. The Jura Mountains - An active foreland fold-and-thrust belt?
 545 Tectonophysics. 321, 381-406.
- 546 Bernet, M., Zattin, M., Garver, J.I., Brandon, M.T., Vance, J.A., 2001. Steady-state
 547 exhumation of the European Alps. *Geology*. 29, 35-38.
- 548 Bigot-Cormier F., 2002. La surrection du massif cristallin externe de l'Argentera (France-
 549 Italie) et ses relations avec la déformation pliocène de la marge nord-Ligure :
 550 arguments thermochronologiques (traces de fission), géomorphologiques et
 551 interprétations de sismique marine. PhD Thesis, University of Nice, France, 352 p.
- 552 Bistacchi, A., Massironi, M., 2000. Post-nappe brittle tectonics and kinematic evolution of the
 553 north-Western Alps: an integrated approach. *Tectonophysics*. 327, 267-292.
- 554 Bogdanoff, S., Michard, A., Mansour, M., Poupeau, G., 2000. Apatite fission track analysis in
 555 the Argentera massif: evidence of contrasting denudation rates in the External
 556 Crystalline Massifs of the Western Alps. *Terra Nova*. 12, 117-125.
- 557 Brandon, M.T., Roden-Tice, M.K., Garver, J.I., 1998. Late Cenozoic exhumation of the
 558 Cascadia accretionary wedge in the Olympic Mountains, Northwest Washington
 559 State. *Geological Society of America Bulletin*. 110, 985-1009.
- 560 Braun, J., 2002. Quantifying the effect of recent relief changes on age-elevation relationships.
 561 *Earth and Planetary Science Letters*. 200, 331-343.
- 562 Braun, J., van der Beek, P., Batt, G., 2006. Quantitative ThermoChronology: Numerical
 563 methods for the interpretation of thermochronological data. Cambridge University
 564 Press, Cambridge. 270 p.
- 565 Bürgi, A., Klötzli, U., 1990. New data in the Evolutionary History of the Ivrea Zone
 566 (Northern Italy). *Bulletin der Vereinigung Schweizerische Petroleum-Geologen und*
 567 *Ingenieur*. 56, 49-69.

- 568 Calais, E., Nocquet, J.-M., Jouanne, F., Tardy, M., 2002. Current strain regime in the Western
569 Alps from continuous Global Positioning System measurements, 1996-2001.
570 *Geology*. 30, 651-654.
- 571 Carpéna, J., 1992. Fission track dating of zircon: zircons from Mont Blanc Granite (French-
572 Italian Alps). *The Journal of Geology*. 100, 411–421.
- 573 Carpéna, J., Caby, R., 1984. Fission track evidence for late Triassic oceanic crust in the
574 French Occidental Alps. *Geology*. 12, 108–111.
- 575 Carpéna, J., Pognante, U., Lombardo, B., 1986. New constraints for the timing of the Alpine
576 metamorphism in the internal ophiolitic nappes from the Western Alps as inferred
577 from fission track data. *Tectonophysics*. 127, 117-127.
- 578 Cederbom, C.E., Sinclair, H.D., Schlunegger, F., Rahn, M.K., 2004. Climate-induced rebound
579 and exhumation of the European Alps. *Geology*. 32, 709-712.
- 580 Champagnac, J.D., Molnar, P., Anderson, R.S., Sue, C., Delacou, B., 2007. Quaternary
581 erosion-induced isostatic rebound in the Western Alps. *Geology*. 35, 195-198.
- 582 Ciancaleoni, L., 2005. Deformation processes during the last stages of the continental
583 collision: the brittle-ductile fault systems in the Bergell and Insubric areas (Eastern
584 Central Alps, Switzerland – Italy). PhD Thesis, University of Neuchâtel,
585 Switzerland, 202 p.
- 586 Debelmas, J., Lemoine, M., 1970. The Western Alps: Paleogeography and Structure. *Earth-*
587 *Science Reviews*. 6, 221-256.
- 588 Dodson, M.H., 1973. Closure temperature in cooling geochronological and petrological
589 systems. *Contributions to Mineralogy and Petrology*. 40, 259-274.
- 590 Ehlers, T.A., Farley, K.A., Rusmore, M.E., Woodsworth, G.J., 2006. Apatite (U-Th)/He
591 signal of large-magnitude accelerated glacial erosion, southwest British Columbia.
592 *Geology*. 34, 765-768.

- 593 Flisch, M., 1986. Die Hebungsgeschichte der oberostalpinen Silvretta-Decke seit der mittleren
594 Kreide. Bulletin der Vereinigung Schweizerische Petroleum-Geologen und
595 Ingenieur. 53, 23-49.
- 596 Fügenschuh, B., Loprieno, A., Ceriani, S., Schmid, S.M., 1999. Structural analysis of the
597 Subbriançonnais and Valais units in the area of Moûtiers, Savoy, Western Alps:
598 paleogeographic and tectonic consequences. International Journal of Earth Sciences.
599 88, 201-218.
- 600 Fügenschuh, B., Schmid, S.M., 2003. Late stages of deformation and exhumation of an
601 orogen constrained by fission track data: A case study in the Western Alps.
602 Geological Society of America Bulletin. 115, 1425-1440.
- 603 Gallagher, K., Brown, R., Johnson, C., 1998. Fission track analysis and its applications to
604 geological problems. Annual Review of Earth and Planetary Sciences. 26, 519-572.
- 605 Gallagher, K., Brown, R., 1999. Denudation and uplift at passive margins: the record on the
606 Atlantic margin of southern Africa. Philosophical Transactions of the Royal Society
607 of London. 357, 835-859.
- 608 Giger, M., 1991. Geochronologische und petrographische Studien an Geröllen und
609 Sedimenten der Gonfolite Lombarda Gruppe (Südschweiz und Norditalien) und ihr
610 Vergleich mit dem alpinen Hinterland. PhD Thesis, University of Bern, Switzerland,
611 227 p.
- 612 Hinderer, M., 2001. Late Quaternary denudation of the Alps, valley and lake fillings and
613 modern river loads. Geodinamica Acta. 14, 231-263.
- 614 Homewood, P., Allen, P.A., Williams, G.D., 1986. Dynamics of the Molasse Basin of western
615 Switzerland, in: Allen, P.A., Homewood, P. (Eds.), Foreland basins. International
616 Association of Sedimentologists Special Publication. 8, 199-217.

- 617 Hunziker, J., Desmons, J., Hurford, A.J., 1992. Thirty-two years of geochronological work in
618 the Central and Western Alps: a review on seven maps. *Mémoire de Géologie* 13,
619 Lausanne, 59 p.
- 620 Hurford, A.J., 1986. Cooling and uplift patterns in the Lepontine Alps, South Central
621 Switzerland and an age of vertical movement of the Insubric fault line. *Contributions*
622 *to Mineralogy and Petrology*. 92, 413-427.
- 623 Hurford, A.J., 1991. Uplift and cooling pathways derived from fission track analysis and mica
624 dating: a review. *Geologische Rundschau*, 80, 349-368.
- 625 Hurford, A.J., Green, P.F., 1982. A user's guide to fission track dating calibration. *Earth and*
626 *Planetary Science Letters*. 59, 343-354.
- 627 Hurford, A.J., Hunziker, J.C., 1985. Alpine cooling history of the Monte Mucrone eclogites.
628 *Schweizerische Mineralogische und Petrographische Mitteilungen*. 65, 325-334.
- 629 Hurford, A.J., Hunziker, J.C., 1989. A revised thermal history for the Gran Paradiso massif.
630 *Schweizerische Mineralogische und Petrographische Mitteilungen*. 69, 319-329.
- 631 Hurford, A.J., Hunziker J.C., Stöckhert, B., 1991. Constraints on the late thermotectonic
632 evolution of the Western Alps: Evidence for episodic rapid uplift. *Tectonics*. 10,
633 758-769.
- 634 Keller, L.M., Hess, M., Fügenschuh, B., Schmid, S., 2005. Structural and metamorphic
635 evolution of the Camughera-Moncucco, Antrona and Monte Rosa units southwest of
636 the Simplon line, Western Alps. *Eclogae geologicae Helvetiae*. 98, 19-49.
- 637 Knaus, A., 1990. Apatit-Spaltspurendatierungen in Rätikon (Arosazone, Östalpen), part 1.
638 Diploma Thesis, University of Tübingen, Germany, 60 p.
- 639 Kuhlemann, J., 2000. Post-collisional sediment budget of circum-Alpine basins (Central
640 Europe). *Memorie di Scienze Geologiche*, Padova. 52, 1-91.

- 641 Kuhlemann, J., Frisch, W., Szekely, B., Dunkl, I., Kazmer, M., 2002. Post-collisional
642 sediment budget history of the Alps: tectonic versus climatic control. *International*
643 *Journal of Earth Sciences*. 91, 818-837.
- 644 Lelarge, L., 1993. Thermochronologie par la méthode des traces de fission d'une marge
645 passive (Dome de Ponta Grossa, SE Brésil) et au sein d'une chaîne de collision
646 (zone externe de l'arc alpin, France). PhD Thesis, University of Grenoble, France,
647 252 p.
- 648 Leloup, P.H., Arnaud, N., Sobel, E.R., Lacassin, R., 2005. Alpine thermal and structural
649 evolution of the highest external crystalline massif: The Mont Blanc. *Tectonics*. 24,
650 TC4002, doi:10.1029/2004TC001676.
- 651 Malusa, M.G., Polino, R., Zattin, M., Bigazzi, G., Martin, S., Piana, F., 2005. Miocene to
652 Present differential exhumation in the Western Alps: Insights from fission track
653 thermochronology. *Tectonics*. 24, TC3004, doi:10.1029/2004TC001782.
- 654 Michalski, I., Soom, M., 1990. The Alpine thermo-tectonic evolution of the Aar and Gotthard
655 massifs, Central Switzerland: Fission track ages on zircons and apatites and K-Ar
656 mica ages. *Schweizerische Mineralogische und Petrographische Mitteilungen*. 70,
657 373-387.
- 658 Molnar, P., 2004. Late Cenozoic Increase in Accumulation Rates of Terrestrial Sediment:
659 How Might Climate Change Have Affected Erosion Rates? *Annual Review of Earth*
660 *and Planetary Sciences*. 32, 67-89.
- 661 Morris, R.G., Sinclair, H.D., Yelland, A.J., 1998. Exhumation of the Pyrenean orogen:
662 implications for sediment discharge. *Basin Research*. 10, 69-85.
- 663 Oberhänsli, R., Bousquet, R., Engi, M., Goffé, B., Gosso, G., Handy, M., Höck, V., Koller,
664 F., Lardeaux, J.-M., Polino, R., Rossi, O.P., Schuster, R., Schwartz, S., Spalla, I.,
665 2004. Metamorphic structure of the Alps, 1:1 000 000, Commission for the

- 666 Geological Map of the World. Mitteilungen der Österreichischen Mineralogischen
667 Gesellschaft. 149.
- 668 Pawlig, S., 2001. Geological Evolution of the Monte Rosa: Constraints from Geochronology
669 and Geochemistry of a Talc-Kyanite-Chloritoid Shear Zone within the Monte Rosa
670 Granite (Monte Rosa Nappe, Italian Western Alps). PhD Thesis, University of
671 Mainz, Germany, 149 p.
- 672 Persaud, M., Pfiffner, O.A., 2004. Active deformation in the eastern Swiss Alps: post-glacial
673 faults, seismicity and surface uplift. *Tectonophysics*. 385, 59-84.
- 674 Pieri, M., Groppi, G., 1981. Subsurface geological structure of the Po Plain. Consiglio
675 Nazionale delle Ricerche, Pubblicazione 414 del Progetto Finalizzato
676 Geodinamica, 23 p.
- 677 Rahn, M.K., 1994. Incipient metamorphism of the Glarus Alps: Petrology of the Tavayanne
678 Greywacke and fission track dating. PhD Thesis, University of Basel, Switzerland,
679 209 p.
- 680 Rahn, M.K., Hurford, A.J., Frey, M., 1997. Rotation and exhumation of a thrust plane: apatite
681 fission track data from the Glarus thrust, Switzerland. *Geology*. 25, 599-602.
- 682 Raymo, M.E., Ruddiman, W.F., 1992. Tectonic forcing of late Cenozoic climate. *Nature*. 359,
683 117-122.
- 684 Ring, U., Brandon, M.T., Willett, S.D., Lister, G.S., 1999. Exhumation processes, in: Ring,
685 U., Brandon, M.T., Lister, G.S., Willett, S.D. (Eds.), *Exhumation Processes: Normal
686 Faulting, Ductile Flow and Erosion*. Geological Society, London, Special
687 Publications. 154, 1-27.
- 688 Rosenbaum, G., Lister, G.S., 2005. The Western Alps from the Jurassic to Oligocene: spatio-
689 temporal constraints and evolutionary reconstructions. *Earth-Science Reviews*. 69,
690 281-306.

- 691 Sabil, N., 1995. La datation par traces de fission : aspects méthodologiques et applications
692 thermochronologiques en contextes alpins et de marge continentale. PhD Thesis,
693 University of Grenoble, France, 238 p.
- 694 Scardia, G., Muttoni, G., Sciunnach, D., 2006. Subsurface magnetostratigraphy of Pleistocene
695 sediments from the Po Plain (Italy): Constraints on rates of sedimentation and rock
696 uplift. *Geological Society of America Bulletin*. 118, 1299-1312.
- 697 Schär, J.P., Reimer, G.M., Wagner, G.A., 1975. Actual and ancient uplift rate in the Gotthard
698 region, Swiss Alps: A comparison between precise levelling and fission track apatite
699 age. *Tectonophysics*. 29, 293-300.
- 700 Schlunegger, F., Hinderer, M., 2001. Crustal uplift in the Alps: why the drainage pattern
701 matters. *Terra Nova*. 13, 425-432.
- 702 Schlunegger, F., Willett, S.D., 1999. Spatial and temporal variations in exhumation of the
703 central Swiss Alps and implications for exhumation mechanisms, in: Ring, U.,
704 Brandon, M.T., Lister, G.S., Willett, S.D. (Eds.), *Exhumation Processes: Normal
705 Faulting, Ductile Flow and Erosion*. Geological Society, London, Special
706 Publications. 154, 157-179.
- 707 Schmid, S.M., Fügenschuh, B., Kissling, E., Schuster, R., 2004. Tectonic map and overall
708 architecture of the Alpine orogen. *Eclogae geologicae Helvetiae*. 97, 93-117.
- 709 Schmid, S.M., Pfiffner, O.A., Froitzheim, N., Schönborn, G., Kissling, E., 1996. Geophysical-
710 geological transect and tectonic evolution of the Swiss-Italian Alps. *Tectonics*. 15,
711 1036-1064.
- 712 Schwartz, S., 2000. La zone piémontaise des Alpes occidentales : un paléo-complexe de
713 subduction. Arguments métamorphiques, géochronologiques et structuraux. PhD
714 Thesis, University of Lyon 1, France, 341 p.

- 715 Seward, D., Ford, M., Bürgisser, J., Lickorish, H., Williams, E.A., Meckel, L.D.III, 1999.
716 Preliminary results of fission track analyses in the Southern Pelvoux area, SE
717 France. 3rd Workshop on Alpine Geological Studies, Memorie di Scienze
718 Geologiche Padova. 51, 25-31.
- 719 Seward, D., Mancktelow, N.S., 1994. Neogene kinematics of the central and Western Alps:
720 Evidence from fission-track dating. *Geology*. 22, 803-806.
- 721 Soom, M.A., 1990. Abkühlungs- und Hebungsgeschichte der Externmassive und der
722 penninischen Decken beidseits der Simplon-Rhone-Linie seit dem Oligozän:
723 Spaltspurdatering and Apatit/Zirkon und K-Ar-Datierungen an Biotit/Muskovit
724 (westliche Zentralalpen). PhD Thesis, University of Bern, Switzerland, 64 p.
- 725 Steiner, H., 1984. Mineralogisch-petrographische, geochemische und isotopengeologische
726 Untersuchungen an einem Meta-Lamprophyr und seinem granodioritischen
727 Nebengestein (Matorello-Gneis) aus der Maggia-Decke. Schweizerische
728 Mineralogische und Petrographische Mitteilungen. 64, 227-259.
- 729 Stephenson, J., Gallagher, K., Holmes, C.C., 2006. Low temperature thermochronology and
730 strategies for multiple samples 2: Partition modelling for 2-D/3-D distributions with
731 discontinuities. *Earth and Planetary Science Letters*. 241, 557-570.
- 732 Stüwe, K., White, L., Brown, R., 1994. The influence of eroding topography on steady-state
733 isotherms. Application to fission track analysis. *Earth and Planetary Science Letters*.
734 124, 63-74.
- 735 Sue, C., Delacou, B., Champagnac, J.-D., Allanic, C., Tricart, P., Burkhard, M., 2007.
736 Extensional neotectonics around the bend of the Western/Central Alps: an overview.
737 *International Journal of Earth Sciences*. 96, 1001-1029.
- 738 Timar-Geng, Z., Grujic, D., Rahn, M., 2004. Deformation at the Leventina-Simano nappe
739 boundary, Central Alps, Switzerland. *Eclogae geologicae Helvetiae*. 97, 265-278.

- 740 Trautwein, B., 2000. Detritus provenance and thermal history of the Rhenodanubian flysch
741 zone: mosaic stones for the reconstruction of the geodynamic evolution of the
742 Eastern Alps. *Tübinger Geowissenschaftliche Arbeiten* 59, 75 p.
- 743 Tricart, P., van der Beek, P., Schwartz, S., Labrin, E., 2007 Diachronous late-stage
744 exhumation across the Western Alpine arc: constraints from apatite fission track
745 thermochronology between the Pelvoux and Dora-Maira Massifs. *Journal of the*
746 *Geological Society, London*. 163, 1-12.
- 747 Trümpy, R., 1960. Paleotectonic evolution of the central and Western Alps. *Bulletin of the*
748 *Geological Society of America* 71: 843-908.
- 749 van der Beek, P., Bourbon, P., 2008. A quantification of the glacial imprint on relief
750 development in the French Western Alps. *Geomorphology* in press.
- 751 van der Beek, P., Robert, X., Mugnier, J.-L., Bernet, M., Huyghe, P., Labrin, E., 2006. Late
752 Miocene-Recent exhumation of the central Himalaya and recycling in the foreland
753 basin assessed by apatite fission track thermochronology of Siwalik sediments,
754 Nepal. *Basin Research*. 18, 413-434.
- 755 Vance, J.A., 1999. Zircon fission track evidence for a Jurassic (Tethyan) thermal event in the
756 Western Alps. In *Fission track Analysis: Theory and Applications*. S. Martin, R.
757 Polino Eds. *Memorie di Scienze Geologiche, Padova*. 51, 473-476.
- 758 Viola, G., 2000. Kinematics and timing of the Periadriatic fault system in the Giudicarie
759 region (central-Eastern Alps). PhD Thesis, n° 13590, ETH Zürich, Switzerland,
760 206 p.
- 761 Wagner, G.A., Miller, D.S., Jäger, E., 1979. Fission track ages on apatite of Bergell rocks
762 from central Alps and Bergell boulders in Oligocene sediments. *Earth and Planetary*
763 *Science Letters*. 45, 355-360.

- 764 Wagner, G.A., Reimer, G.M., 1972. Fission track tectonics: The tectonic interpretation of
765 fission track apatite ages. *Earth and Planetary Science Letters*. 14, 263-268.
- 766 Wagner, G.A., Reimer, G.M., Jäger, E., 1977. Cooling ages derived by apatite fission track,
767 mica Rb-Sr and K-Ar dating: the uplift and cooling history of the Central Alps.
768 *Memorie di Scienze Geologiche, Padova*. 30, 1-27.
- 769 Watson, D., 1999. The natural neighbor series manuals and source codes. *Computers and*
770 *Geosciences*. 25, 463-466.
- 771 Weh, M., 1998. Tektonische Entwicklung der penninischen Sediment-Decken in Graubünden
772 (Prättigau bis Oberhalbstein). PhD Thesis, University of Basel, Switzerland, 230 p.
- 773 Willett, S.D., Schlunegger, F., Picotti, V., 2006. Messinian climate change and erosional
774 destruction of the central European Alps. *Geology*. 34, 613-616.
- 775 Zhang, P., Molnar, P., Downes, W.R., 2001. Increased sedimentation rates and grain sizes 2-4
776 Myr ago due to the influence of climate change on erosion rates. *Nature*. 410, 891-
777 897.
- 778

779 **Figure captions**

780

781 **Figure 1.** Evolution of sedimentation rates through time, reconstructed from the preserved
782 volume of sediments originating from the Western and the Eastern Alps, respectively
783 (modified from Kuhlemann et al., 2002).

784

785 **Figure 2.** (a) Simplified geologic map of the Western Alps (modified from Schmid et al.,
786 2004). The study area (shown by bold outline) covers the geological units with the highest
787 density of fission track ages (cf. Figure 3), limited to the east by the Austroalpine Silvretta
788 nappe boundary at about 9°55' E. (b) Cross-section following north-south transect A-B across
789 the central Swiss Alps (modified from Schmid et al., 1996).

790

791 **Figure 3-a.** Map of 635 AFT ages from the Western Alps, interpolated using a natural-
792 neighbor algorithm. Morphotectonic regions and units referred to in the text: (1) Argentera,
793 (2) Ecrins, (3) Belledonne, (4) Mont-Blanc, (5) Aar, (6) Chur area, (7) Gran Paradiso, (8)
794 Sesia, (9) Dent-Blanche, (10) Penninic thrust, (11) Simplon fault, (12) Periadriatic line. AFT
795 data are compiled from Bigot-Cormier 2002; Bogdanoff et al. 2000; Bürgi and Klötzli 1990;
796 Carpéna and Caby 1984; Carpéna 1992; Ciancaleoni 2005; Flisch 1986; Fügenschuh and
797 Schmid 2003; Fügenschuh et al. 1999; Giger 1991; Hunziker et al. 1992; Hurford and
798 Hunziker 1989; Hurford 1986; Hurford et al. 1991; Keller et al. 2005; Knaus 1990; Lelarge
799 1993; Leloup et al. 2005; Malusà et al. 2005; Michalski and Soom 1990; Pawlig 2001; Rahn
800 et al. 1997; Sabil 1995; Schär et al. 1975; Schwartz 2000; Seward and Mancktelow 1994;
801 Seward et al. 1999; Soom 1990; Steiner 1984; Timar-Geng et al. 2004; Trautwein 2000;
802 Tricart et al. 2006; Viola 2000; Wagner and Reimer 1972; Wagner et al. 1977; Wagner et al.

803 1979; Weh 1998; as well as unpublished ages provided by M. Ford, D. Seward and our own
804 data.

805

806 **Figure 3-b.** Map of 296 interpolated ZFT ages from the Western Alps. Numbers are as in
807 Figure 3-a. ZFT data are compiled from Bernet et al. 2001; Bigot-Cormier 2002; Bürgi and
808 Klötzli 1990; Carpéna 1992; Carpéna et al. 1986; Ciancaleoni 2005; Flisch 1986; Fügenschuh
809 and Schmid 2003; Fügenschuh et al. 1999; Giger 1991; Hunziker et al. 1992; Hurford and
810 Hunziker 1985; Hurford and Hunziker 1989; Hurford 1986; Hurford et al. 1991; Keller et al.
811 2005; Michalski and Soom 1990; Rahn 1994; Schwartz 2000; Seward and Mancktelow 1994;
812 Seward et al. 1999; Soom 1990; Vance 1999; Weh 1998; as well as unpublished ages
813 provided by M. Ford, D. Seward and our own data.

814

815 **Figure 3-c.** Interpolated map of 258 mean apatite fission-track lengths (μm) from the Western
816 Alps. Short mean lengths ($< 13 \mu\text{m}$) indicate slow passage of the sample through the AFT
817 partial annealing zone, indicative of a slow exhumation rate. Long mean track lengths, in
818 contrast, indicate rapid exhumation. Note the strong spatial overlap between mean track
819 lengths $>13 \mu\text{m}$ and AFT ages $<\sim 10 \text{ Ma}$ (Figure 3-a), particularly in the Simplon and Chur
820 areas, as well as more generally in the Mont-Blanc-Ecrins and the Argentera massifs.

821 Numbers are as in Figure 3-a. Apatite fission-track lengths compiled from Bigot-Cormier
822 2002; Bürgi and Klötzli 1990; Ciancaleoni 2005; Giger 1991; Hunziker et al. 1992; Hurford
823 and Hunziker 1989; Hurford 1986; Hurford et al. 1991; Knaus 1990; Malusà et al. 2005;
824 Michalski and Soom 1990; Pawlig 2001; Rahn et al. 1997; Sabil 1995; Seward and
825 Mancktelow 1994; Seward et al. 1999; Soom 1990; Timar-Geng et al. 2004; Trautwein 2000;
826 Tricart et al. 2006; Wagner & Reimer 1972; as well as our own unpublished data.

827

828 **Figure 4.** Variation of exhumation rate (E_r) through time, calculated from samples with
 829 paired AFT and ZFT ages. Samples with both ages younger than 35 Ma (i.e., Alpine cooling
 830 ages) are used to calculate an initial rate during the time between closure of the ZFT and AFT
 831 thermochronometers and a final rate for the time since closure of the AFT system (see text for
 832 details). The color scale presents the ratio between final and initial exhumation rates and
 833 enables to distinguish between localities where average exhumation rates have accelerated
 834 (ratio > 1), remained steady (ratio ≈ 1) or decelerated (ratio < 1) after AFT closure. Data
 835 points are labeled by their AFT age. Data origin is given in the legends of Figure 3-a and 3-b.
 836

837 **Figure 5.** Generic sketch of AFT isoage surface concept. (a) Denudation (i.e., removal of
 838 material) occurring between times t_1 and t_2 over the present day topography is reflected by the
 839 migration of shallow isotherms, downwards with respect to the exhuming rock mass such that
 840 a rock particle is cooled during exhumation (see definitions in Ring et al., 1999). The 120 - 60
 841 °C AFT partial annealing zone is shifted downwards, and so are the AFT closure temperature
 842 (the temperature at which the first track is recorded) and the AFT closure surface (the surface
 843 linking all samples crossing the closure temperature at a given moment). (b) Former closure
 844 surfaces become isoage surfaces, younging downwards and intersecting the topography.
 845

846 **Figure 6.** Steps toward the interpolation of isoage surfaces. A neighborhood search of
 847 significant age-elevation relationships (AER) is performed within 3 km around each data
 848 point (a, b). If the correlation coefficient between age and elevation is not statistically
 849 significant at the 95 % confidence level (b), the radius for selection of points is increased
 850 stepwise up to a maximum of 15 km (c). The A_0 and A_1 parameters defining the regression
 851 lines are used to interpolate the elevation of isoage surfaces between 1 Myr before the oldest
 852 age selected (A_{max}) and 1 Myr after the youngest age selected (A_{min}). Finally, isoage surfaces

853 are obtained by interpolation of isoage point arrays combining the results of neighborhood
854 AER search and the elevation of isoage contours (d). The figure shows a zoom of the
855 Lepontine area and the sources of data points are as in Figure 3a.

856

857 **Figure 7.** Six examples of isoage surfaces among the 13 obtained between 14 and 2 Ma.
858 Following a natural-neighbor interpolation between isoage points, the grid is clipped with a
859 mask at 15 km to reduce the number of pixels located far from any source of information. The
860 color scale represents the elevation in meters above sea level (note that the scale is different
861 for each panel). The overall elevation of old isoage surfaces (e.g., 11 Ma; 14 Ma) is higher
862 than the elevation of younger isoage surfaces (2 Ma; 4 Ma) which is in agreement with the
863 generic sketch in Figure 5.

864

865 **Figure 8.** Areas with continuous isoage surface coverage. Eight areas with isoage surfaces
866 covering 4 to 10 Myr were obtained by comparing the area covered by the 13 isoage surfaces
867 obtained between 14 and 2 Ma (Figure 6). Different periods of time are documented in
868 different areas, as indicated in the legend, depending on the ages accessible at outcrop.

869

870 **Figure 9.** Calculation of denudation rate from the elevation difference of isoage surfaces. (a)
871 Map of the elevation difference between the 5 and 4 Ma isoage surfaces. (b) In this example,
872 values of elevation difference are extracted from the area of continuous isoage surface
873 coverage located on the Mont-Blanc massif (area 4 in Figure 8), and plotted in a frequency
874 histogram. The pixels with a negative value (in black on the map) cannot be used to infer
875 denudation rates and are discarded. The average distance between isoage surfaces is
876 calculated over the remaining histogram and considered to be equivalent to the amount of
877 exhumation affecting the Mont-Blanc area during the corresponding period.

878

879 **Figure 10.** Comparison between the estimates of average denudation rate (recorded in
880 sediment volume) and exhumation rate (using AFT isoage surfaces, this study) over the
881 Western Alps. The average Western Alps denudation rate calculated by Kuhlemann (2000) is
882 the ratio between the peri-Alpine sedimentation rates (Figure 1) and the provenance area. The
883 exhumation rate was estimated over 8 regions of the Western Alps by the isoage surface
884 technique (Figures 5 to 9). Both the envelope of exhumation trend and the denudation curve
885 show an increase centered around 5 Ma. See sections 6.3. and 6.4. for a discussion of the
886 features observed in exhumation rate trends.

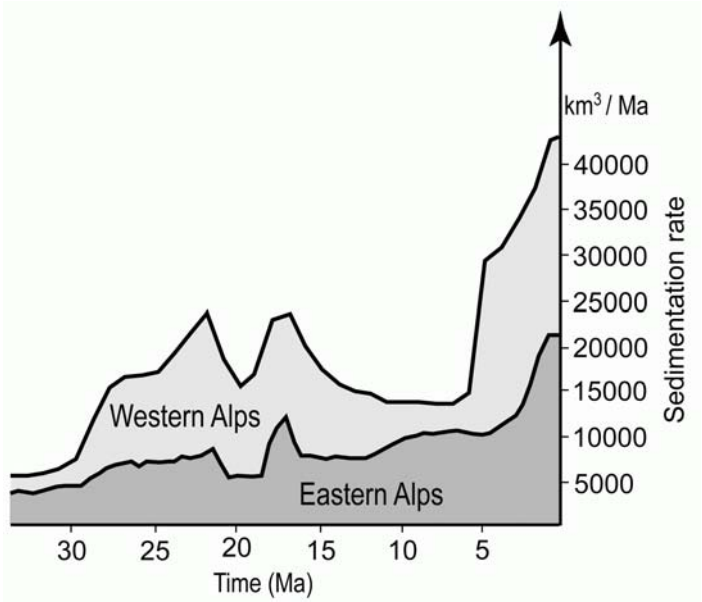


Figure 1

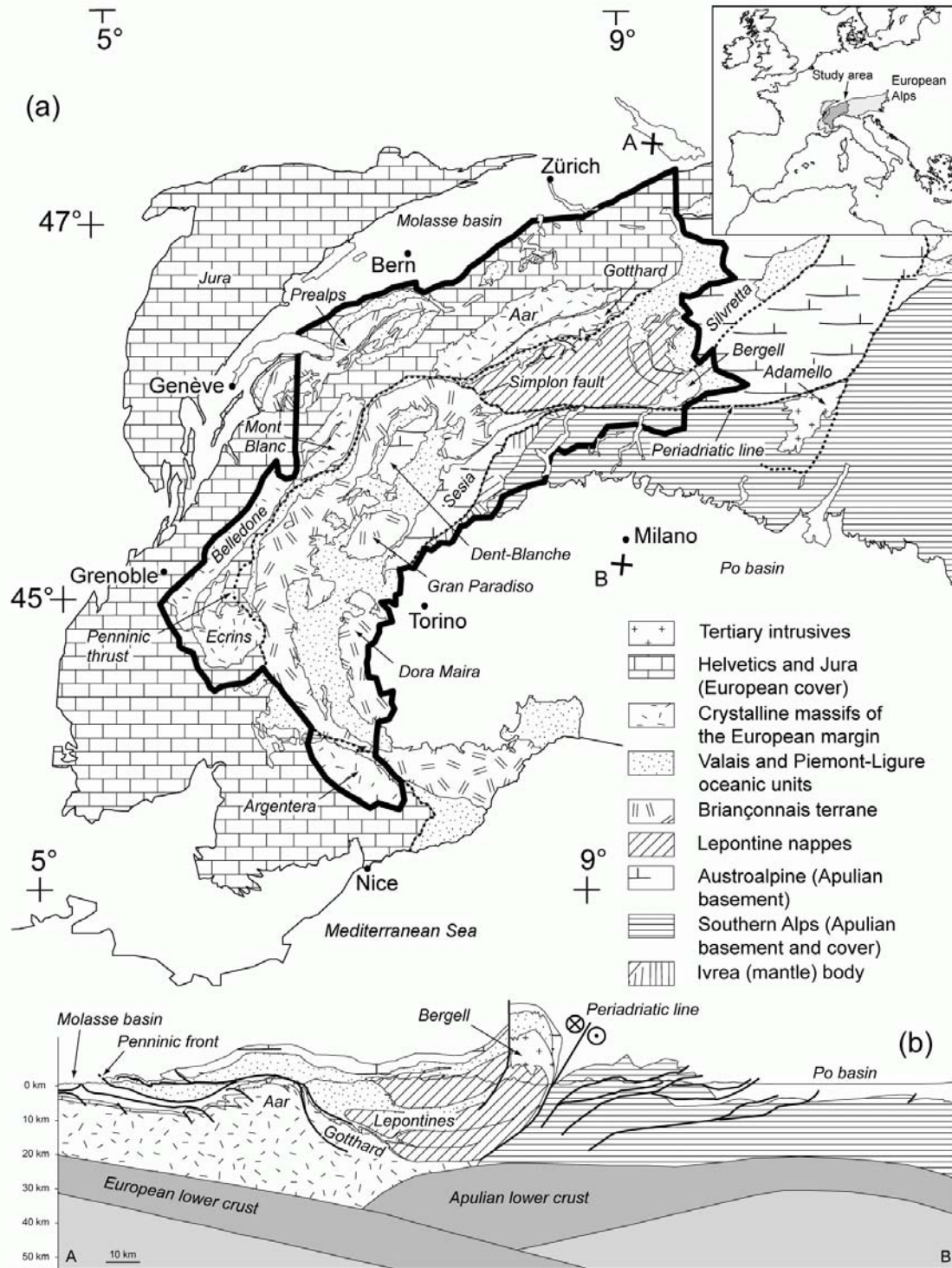


Figure 2

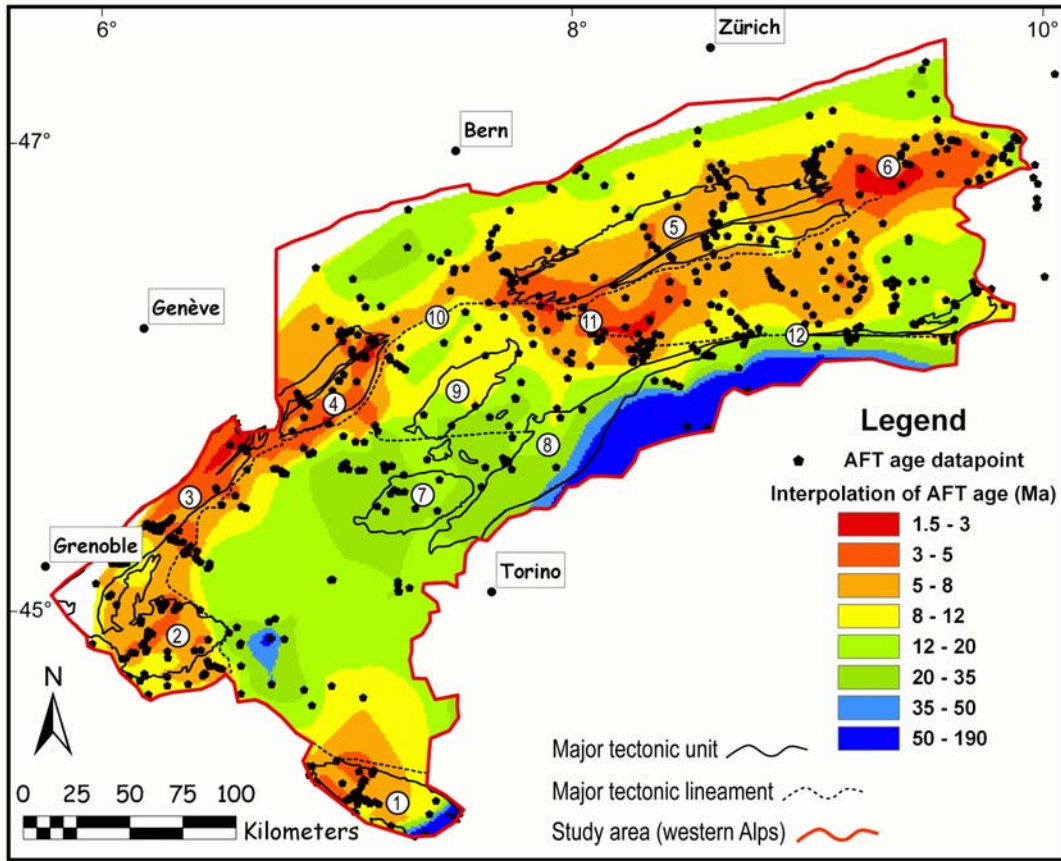


Figure 3-a

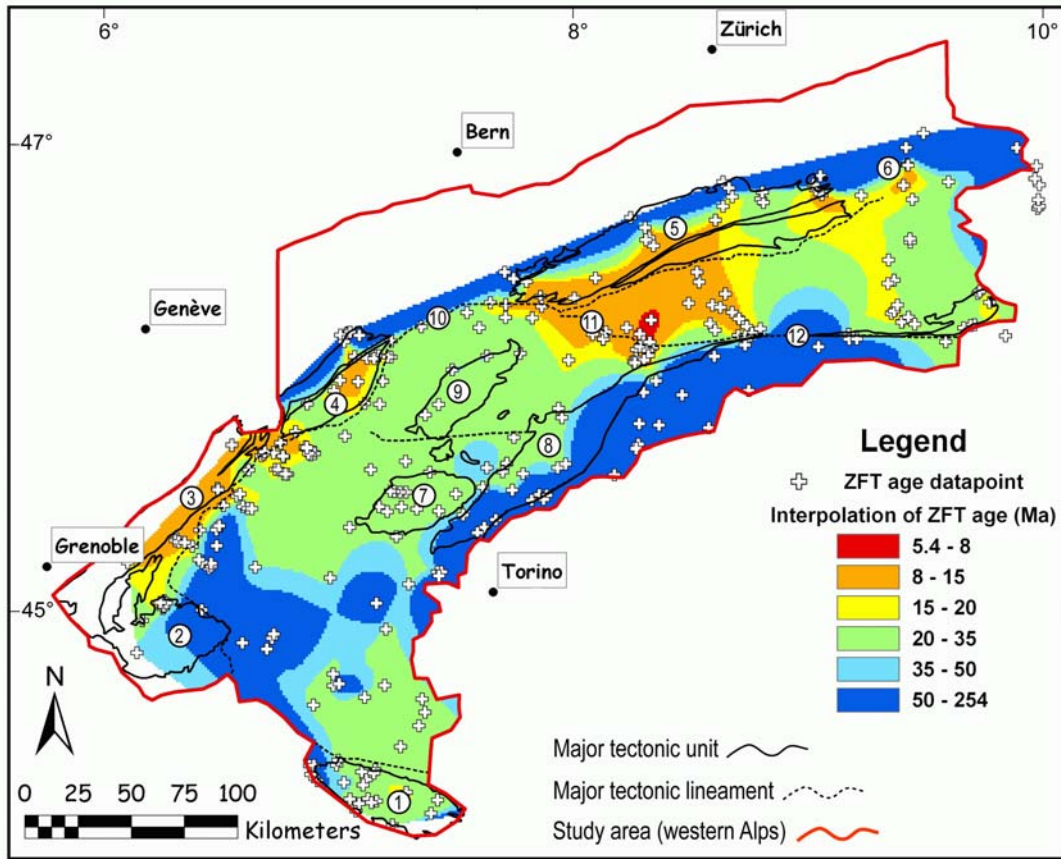


Figure 3-b

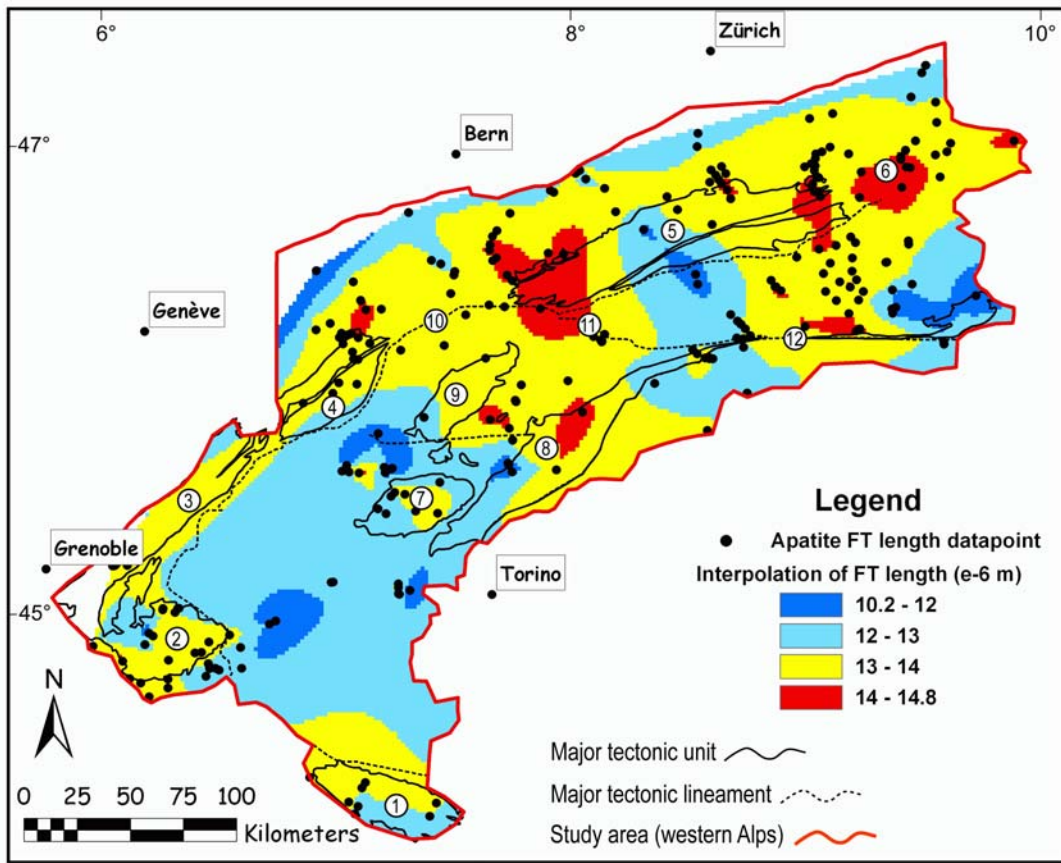


Figure 3-c

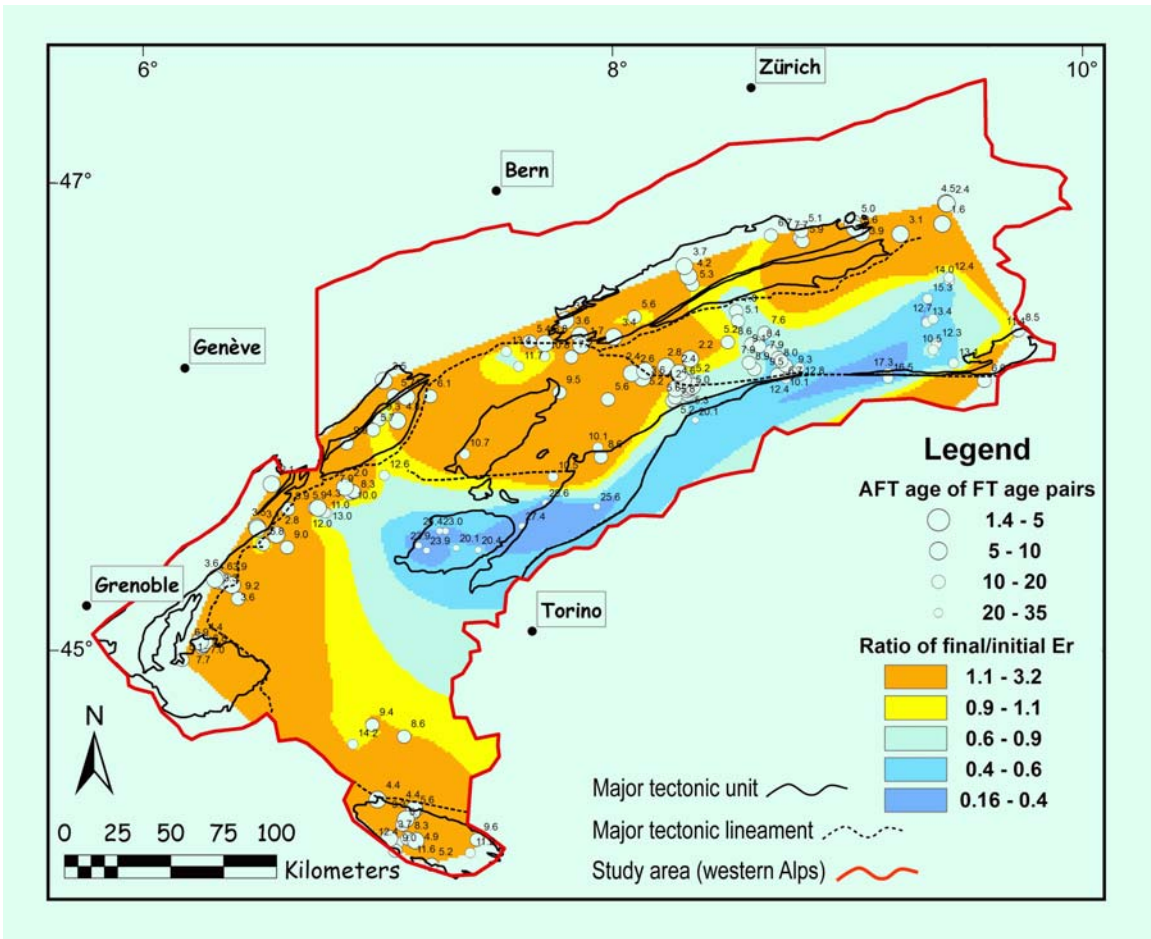


Figure 4

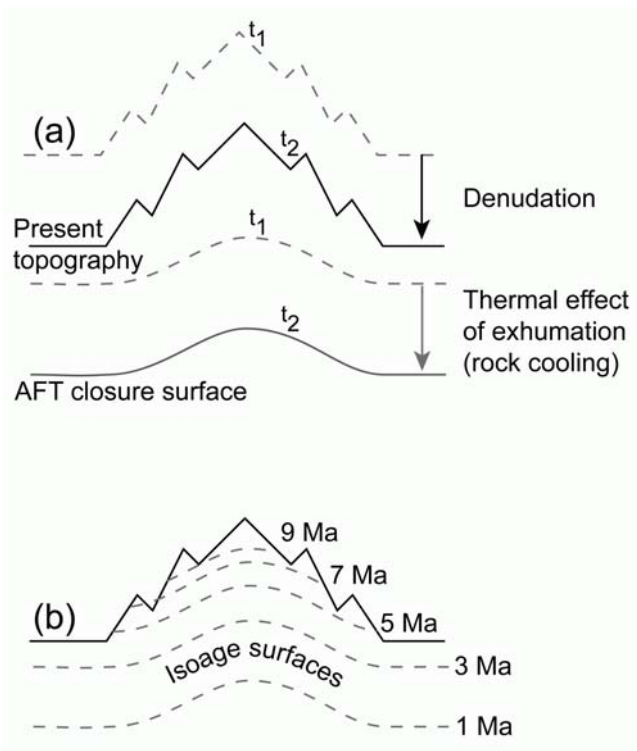


Figure 5

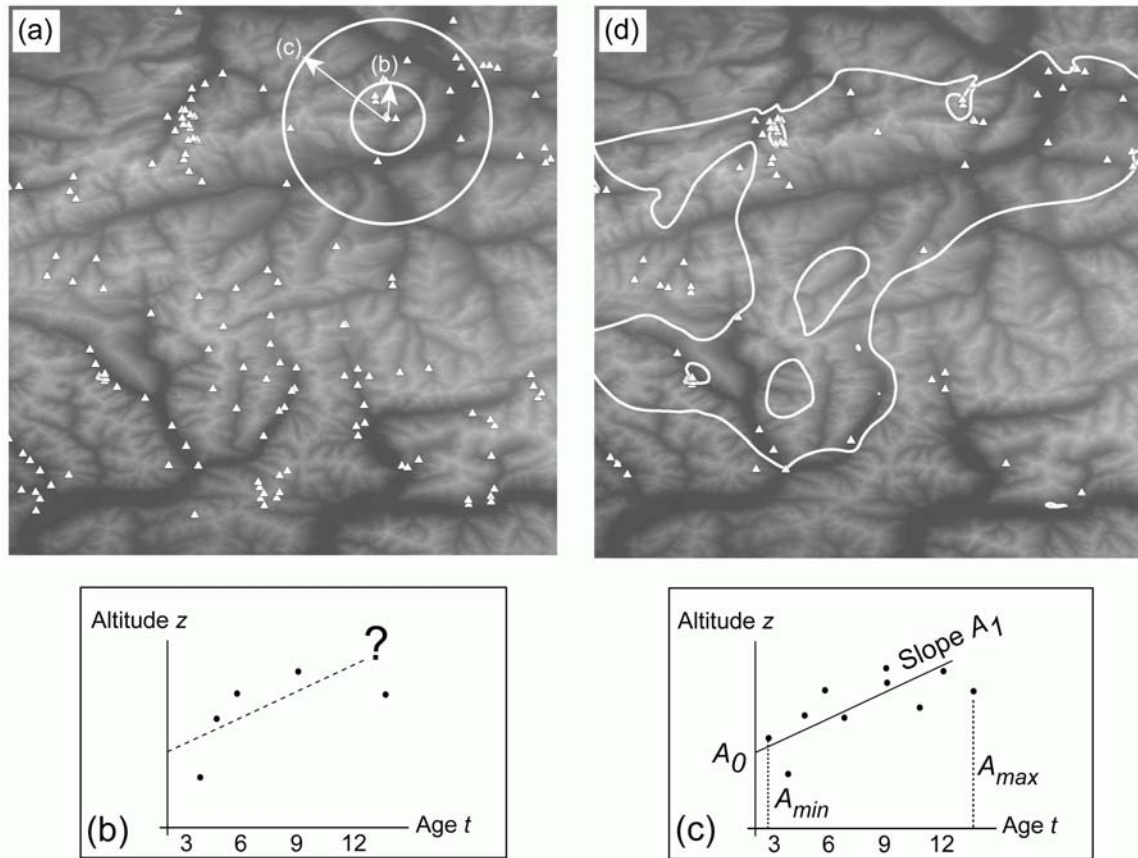


Figure 6

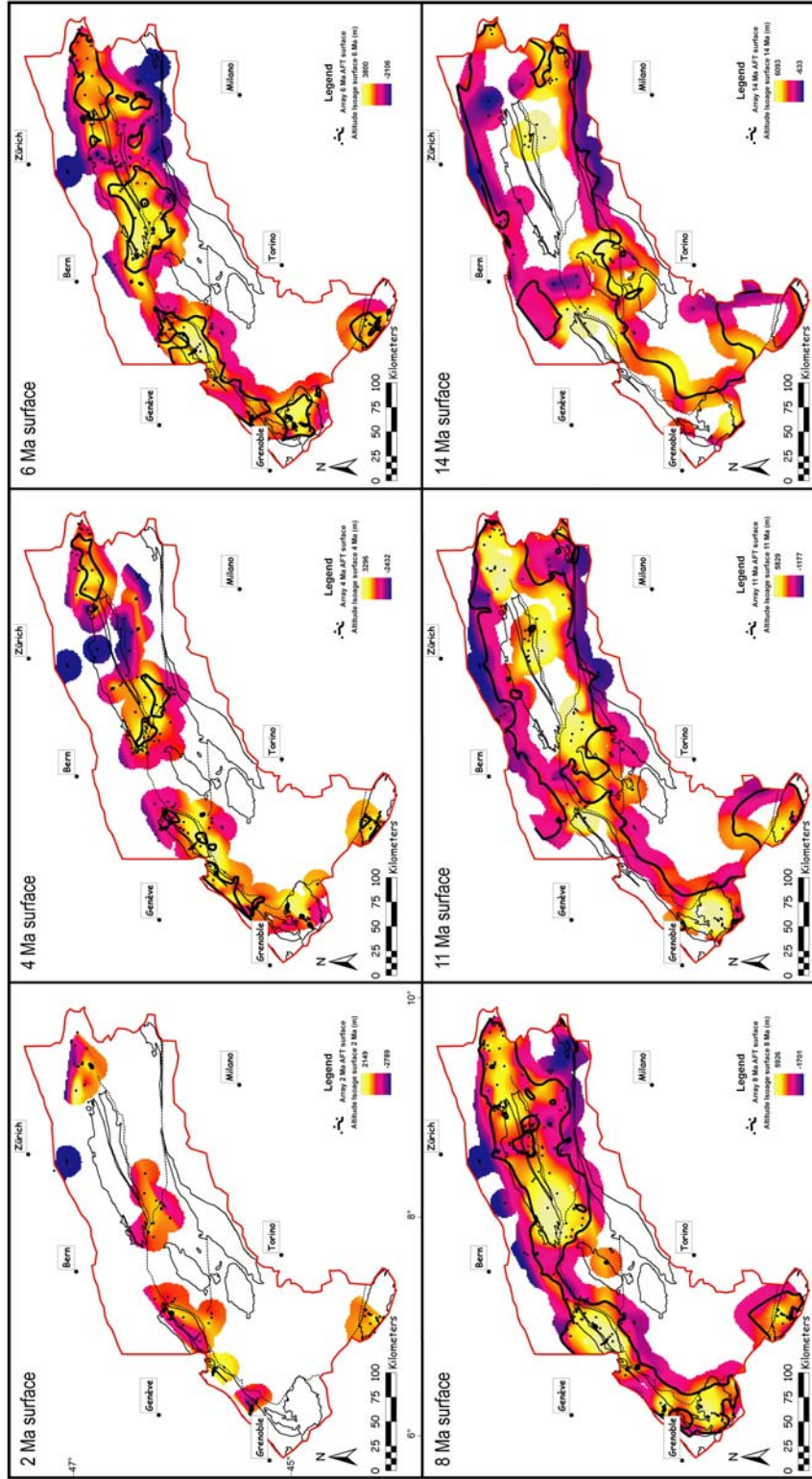


Figure 7

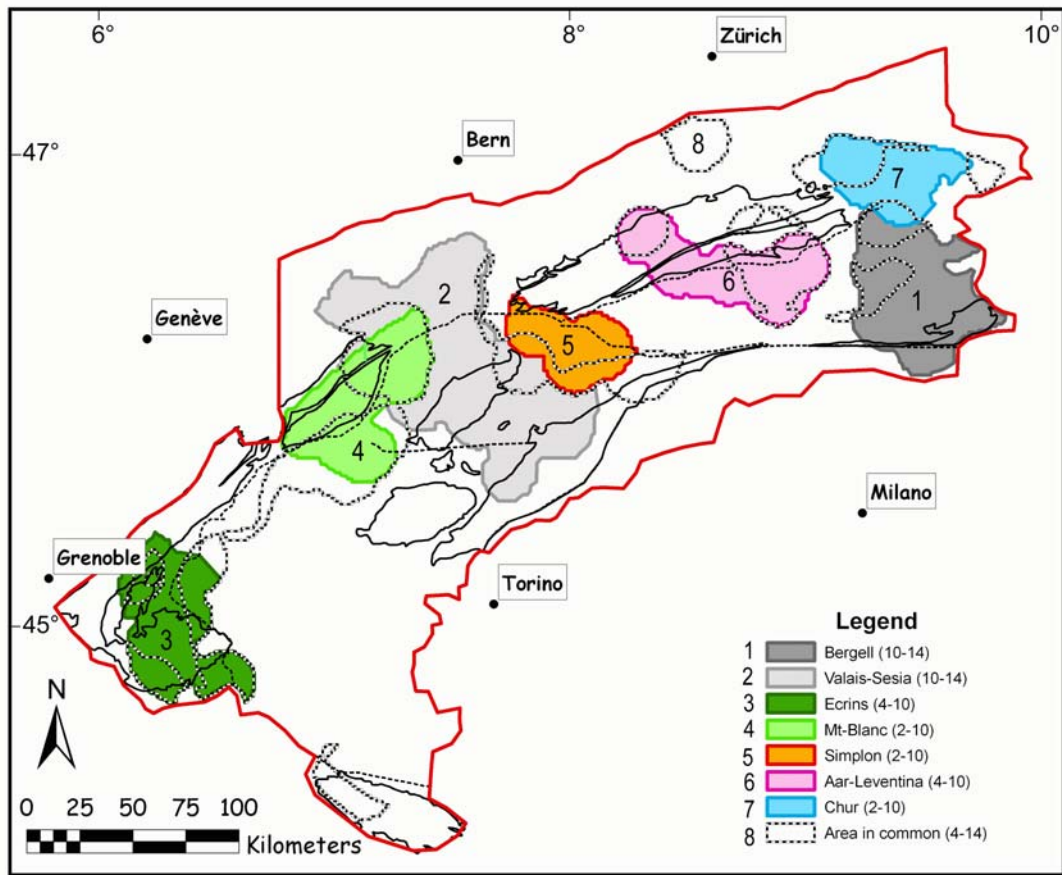


Figure 8

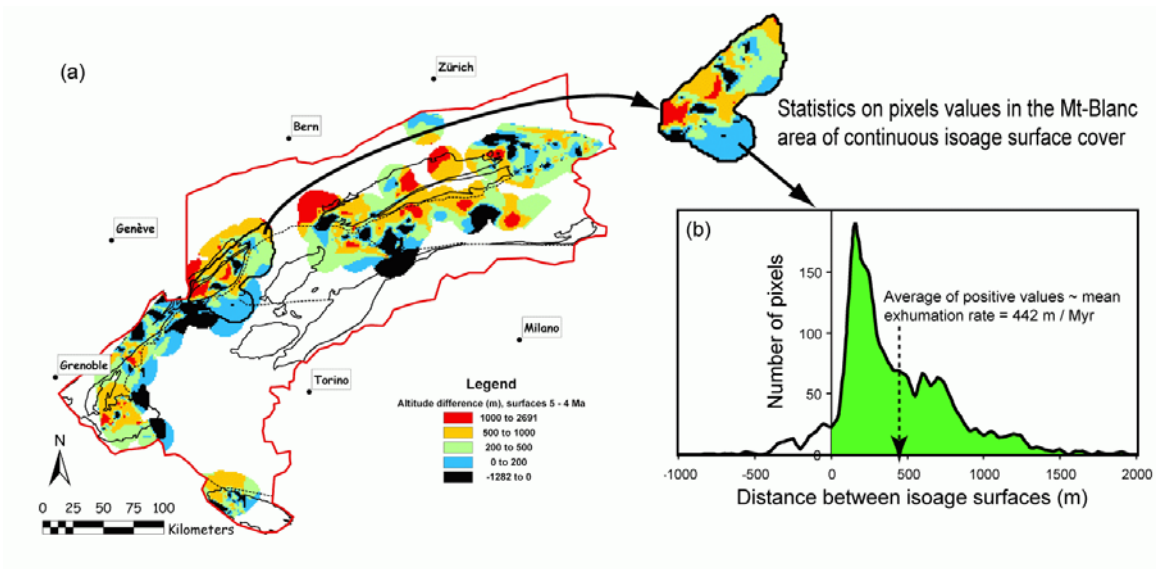


Figure 9

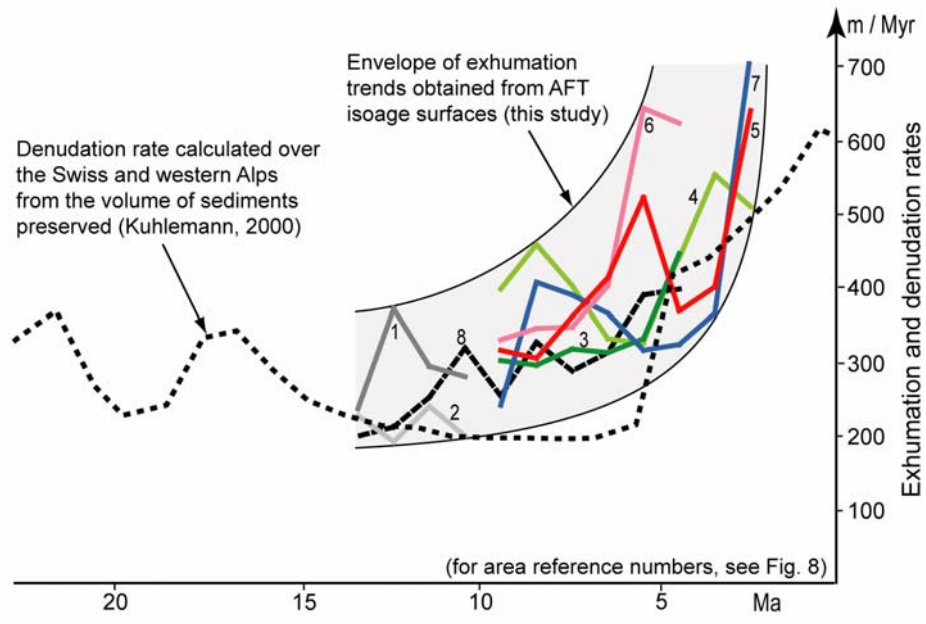


Figure 10